Supporting Information

Nanocomposite Hybrid Biomass Hydrogels as Flexible Strain Sensors with Self-Healing Ability in Harsh Environments

Qichao Fan, Yu Nie, Qing Sun, Wenxiang Wang, Liangjiu Bai,* Hou Chen,* Lixia Yang, Huawei Yang, Donglei Wei

School of Chemistry and Materials Science, Ludong University; Key Laboratory of High Performance and Functional Polymer in the Universities of Shandong Province; Collaborative Innovation Center of Shandong Province for High Performance Fibers and Their Composites, Yantai 264025, China.

Corresponding authors:

Liangjiu Bai, *E-mail: bailiangjiu@ldu.edu.cn

Hou Chen, *E-mail: chenhou@ldu.edu.cn

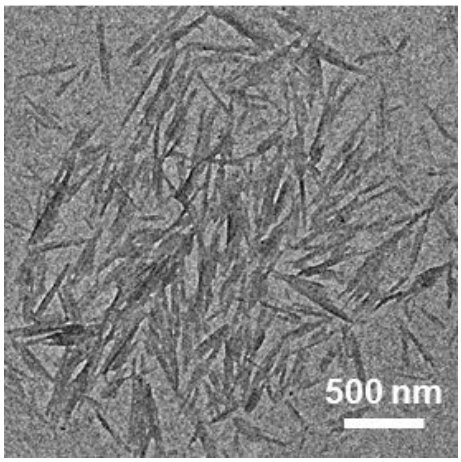

Figure S1. TEM image of CNCs (the length and diameter of CNCs were estimated from at least 100 samples and the data was shown as mean ± standard deviation).

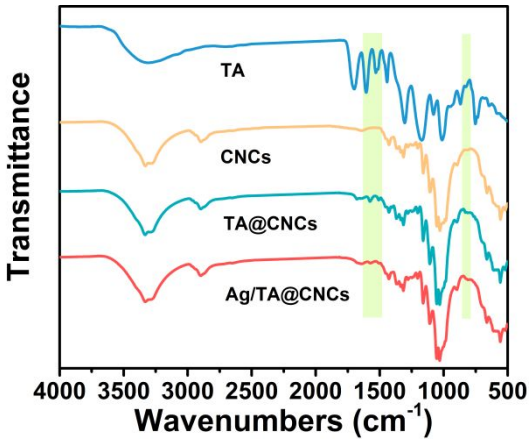

Figure S2. FT-IR spectra of TA, CNCs, TA@CNCs, and Ag/TA@CNCs.

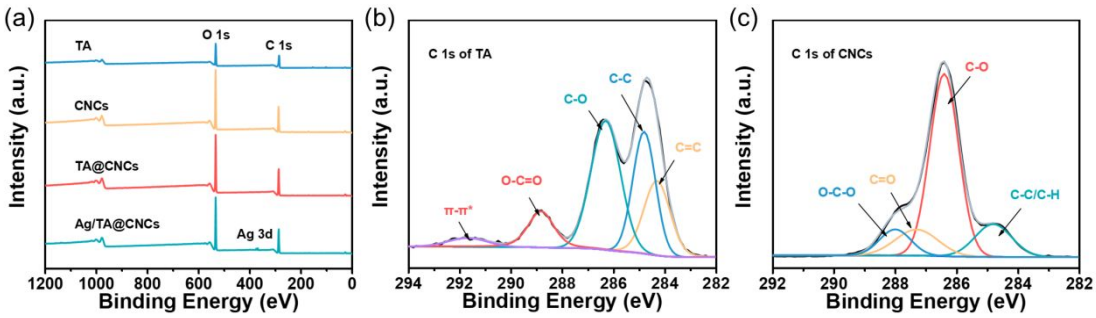

Figure S3. (a) XPS survey spectra of TA, CNCs, TA@CNCs, and Ag/TA@CNCs. C 1s high-resolution XPS spectra of (b) TA and (c) CNCs.

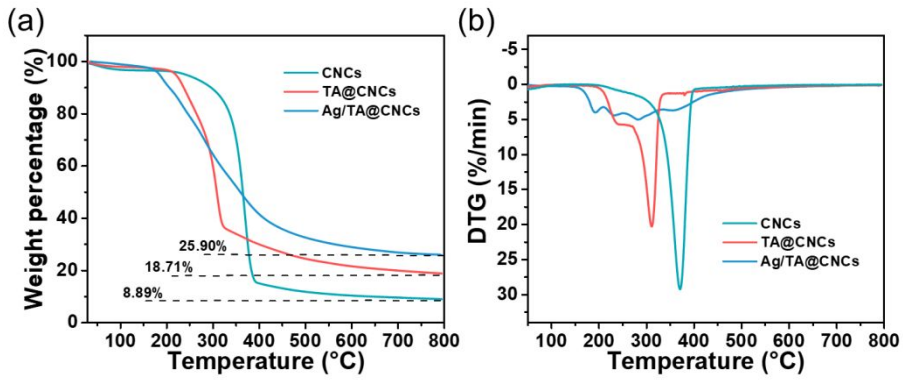

Figure S4. (a) TGA and (b) DTG curves of CNCs, TA@CNCs, and Ag/TA@CNCs.

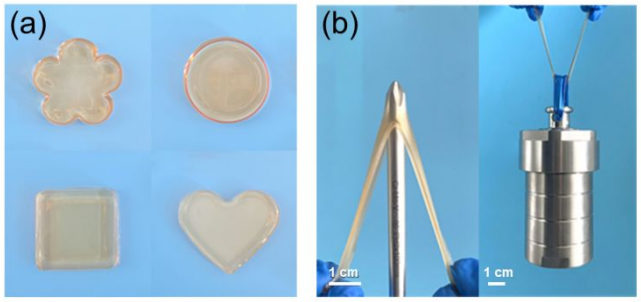

Figure S5. (a) Optical photographs of hydrogels in various shapes. (b) Performance tests of hydrogels with stretching and loading.

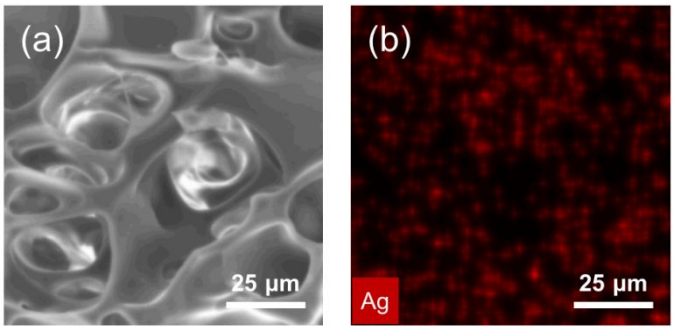

Figure S6. EDS elemental mapping of gel-$C_{0.2}L_{40}$: (a) SEM cross-sectional image and (b) Ag element distribution map.

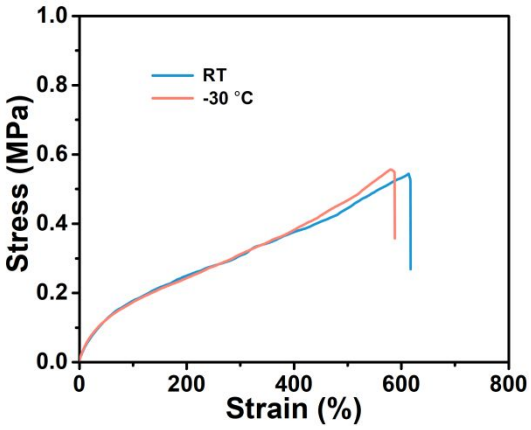

Figure S7. Stress-strain curves of gel-$C_{0.2}L_{40}$ at room temperature and -30 °C.

Table S1. The mechanical properties and self-healing efficiency of different hydrogel samples (the maximum stress, maximum strain, and self-healing efficiency of the samples were tested at least three times and the data was shown as mean ± standard deviation).

Samples	**Max stress (MPa)**	**Max strain (%)**	**Self-healing efficiency (%)**
gel-C_0L_{40}	0.45±0.03	613.2±17.0	71.4±4.6
gel-$C_{0.1}L_{40}$	0.55±0.02	594.8±9.0	83.5±3.3
gel-$C_{0.2}L_{40}$	0.69±0.01	557.5±12.2	88.3±5.0
gel-$C_{0.3}L_{40}$	0.60±0.03	547.2±13.6	86.8±2.5
gel-$CNCs_{0.2}L_{40}$	0.51±0.03	630.3±20.8	80.5±5.5
gel-TA@$CNCs_{0.2}L_{40}$	0.68±0.02	564.3±15.6	88.6±3.6

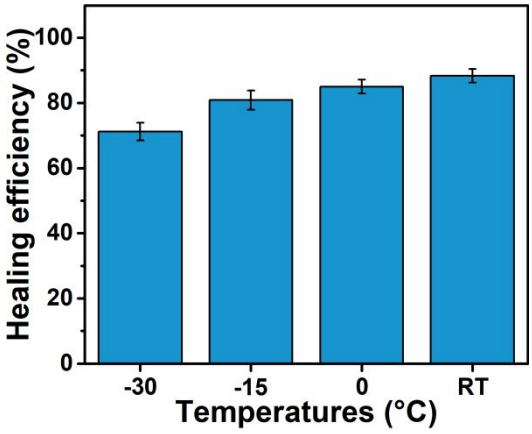

Figure S8. Self-healing efficiency of gel-$C_{0.2}L_{40}$ at -30 °C, -15 °C, 0 °C, and room temperature.

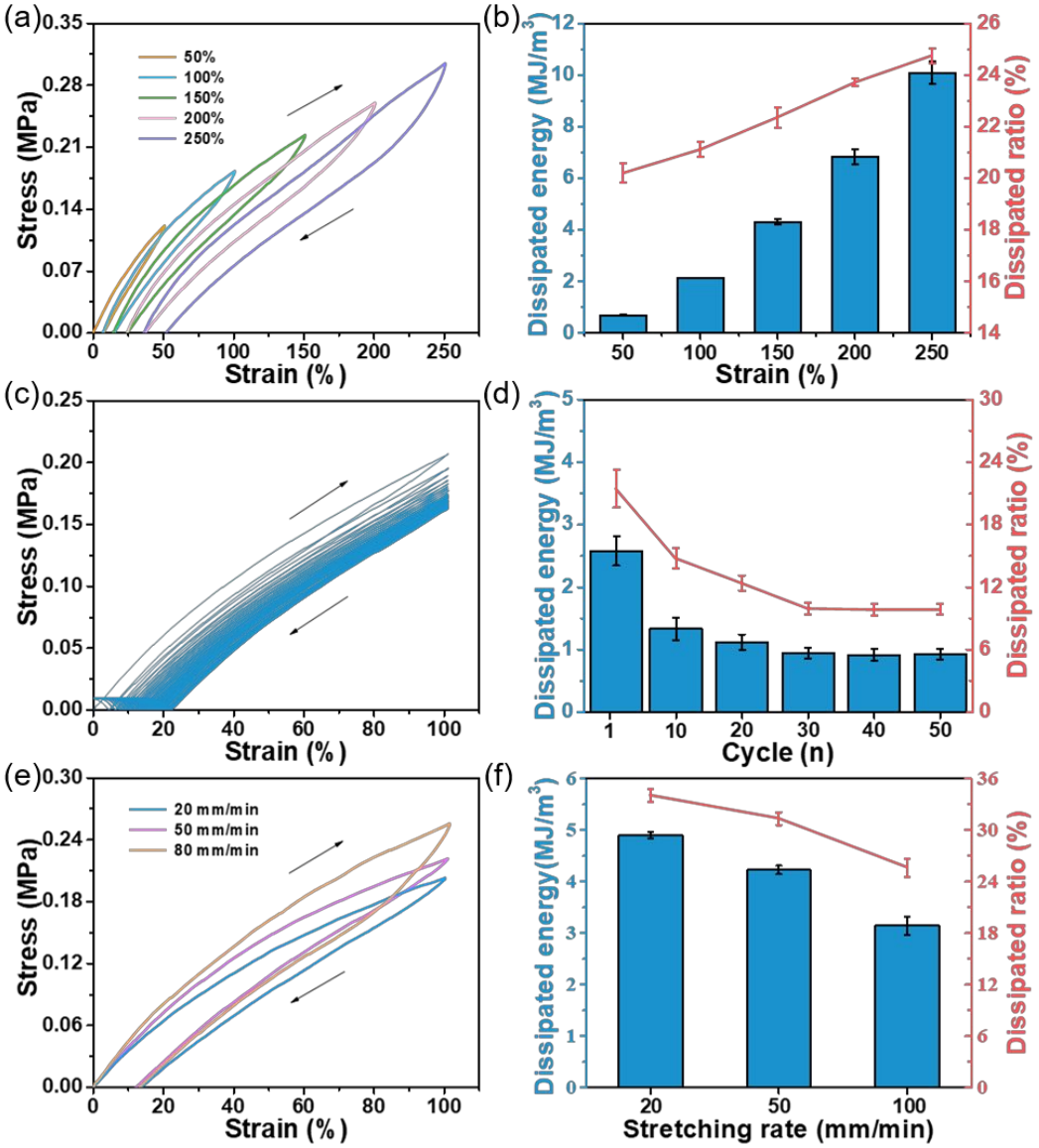

Figure S9. (a-b) Loading−unloading tests of gel-$C_{0.2}L_{40}$ under different strain of 50%, 100%, 150%, 200%, and 250%. (c-d) Fifty successive cyclic loading-unloading tests of gel-$C_{0.2}L_{40}$ at 100% strain. (e-f) Loading−unloading tests of gel-$C_{0.2}L_{40}$ under different tensile rates of 20, 50, and 80 mm/min.

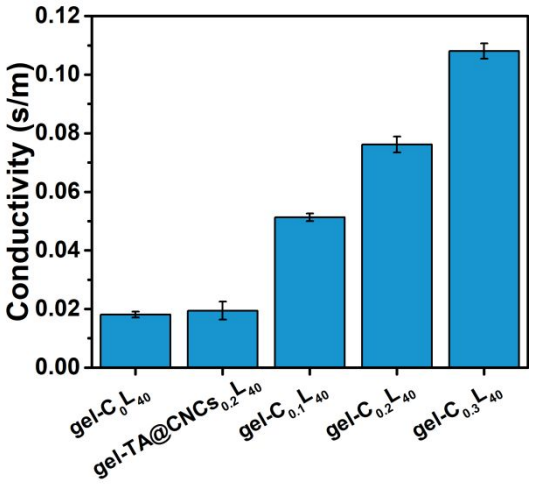

Figure S10. Conductivity of gel-C_0L_{40}, gel-TA@$CNCs_{0.2}L_{40}$, gel-$C_{0.1}L_{40}$, gel-$C_{0.2}L_{40}$ and gel-$C_{0.3}L_{40}$.

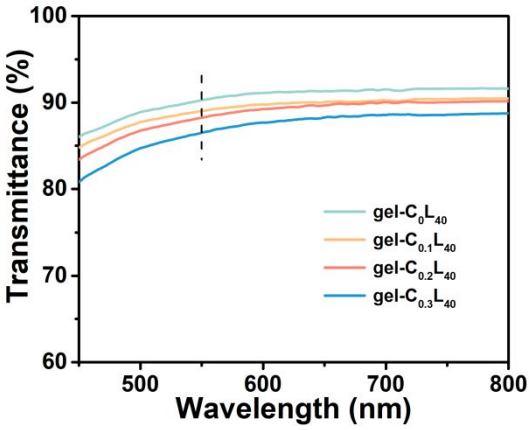

Figure S11. UV-vis transmittance of the gel-C_0L_{40}, gel-$C_{0.1}L_{40}$, gel-$C_{0.2}L_{40}$, and gel-$C_{0.3}L_{40}$ (thickness: 1 mm).

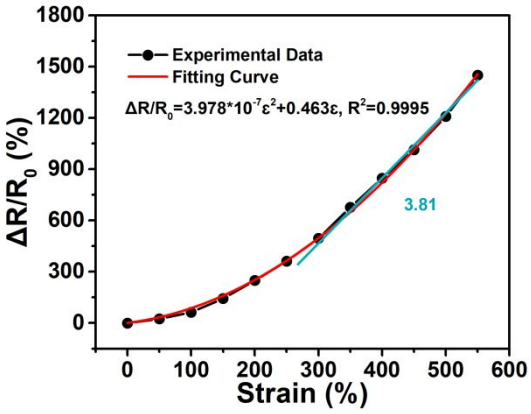

Figure S12. The line-fitting GF factor curves of gel-TA@$CNCs_{0.2}$.

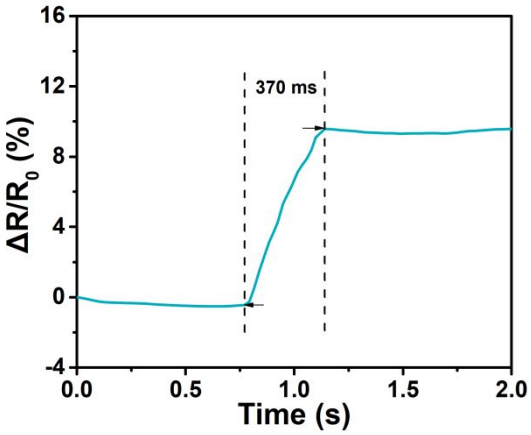

Figure S13. The response time curve of the gel-TA@CNCs$_{0.2}$.